Dynamic Characteristics of TAIPEI 101 Skyscraper from Rotational and Translation Seismometers

Yaochieh Chen[1,2], Philippe Guéguen[2], Kate Huihsuan Chen[*1], Chin-Jen Lin[3], Chin-Shang Ku[3], Win-Gee Huang[3], Bor-Shouh Huang[3], and Kou-Cheng Chen[3]

ABSTRACT

Continuous data streams from translational and rotational seismometers installed in TAIPEI 101 enable monitoring of the natural frequencies on different time scales. Using the 2014 seismic data recorded on the 90th floor of this high-rise building and the meteorological data from a weather station located just 1 km away, we explored the characteristics and controlling factors of the ambient vibrations in TAIPEI 101. Using the random decrement technique, the three modal frequencies in translation were identified as 0.15 Hz (F1), 0.43 Hz (F2), and 0.78 Hz (F3). For rotation around the vertical axis, the modal frequencies were 0.23 Hz (R1), 0.59 Hz (R2), and 0.93 Hz (R3). In translation, TAIPEI 101 exhibits a trend of increasing modal frequency with increasing temperature but decreasing modal frequency with increasing wind velocity. The trend with temperature is reversed in rotation motion. The different frequency versus temperature relationship seen for rotational and translational motion demonstrates the importance of introducing rotational motion analysis into structural health monitoring. The change in modal frequencies were also found to decrease with growing amplitude. It is intriguing that F1 exhibits a weaker dependency with amplitude with respect to the higher modes, which may be associated with the suppression of F1 vibration caused by the damper installed in TAIPEI 101. Other than long-term (seasonable) variation, we also highlight the hourly variation of the first-mode amplitude throughout a day by comparing with weather and mobility data. Other than the atmospheric conditions that strongly influence the modal frequencies in long-term behavior, we found that human activities may play an important role in the short-term vibration characteristics of the building.

KEY POINTS

- We explored the characteristics and controlling factors of the ambient vibrations in TAIPEI 101.
- Temperature, wind speed, and human activity are keys for the variation of the modal frequencies.
- We demonstrated the importance of introducing rotational motion analysis into structural health monitoring.

Supplemental Material

INTRODUCTION

Processing full-scale data from real buildings is valuable for strengthening the science behind building response prediction and structural health monitoring. With the increasing quantity and quality of building instrumentation, great advances have been made over the past two decades in our understanding of building behavior subjected to excitation by strong to weak motions (e.g., earthquakes and ambient vibrations). Because the modal parameters (resonance frequencies and damping) depend on the elastic properties of the structure, they are commonly regarded as useful tools for postearthquake assessment of building damage (Fukuwa *et al.*, 1996; Clinton *et al.*, 2006; Vidal *et al.*, 2014) and more generally for structural health monitoring (e.g., Farrar and Worden, 2007). It has been found that the structural dynamic parameters are sensitive to (1) permanent changes in building structure due to the defects and cracks caused by earthquakes or strong external loading

1. Department of Earth Sciences, National Taiwan Normal University, Taipei, Taiwan, https://orcid.org/0000-0001-6024-278X (YC); https://orcid.org/0000-0002-5164-9681 (KHC); 2. ISTerre, Universitaire de Grenoble, Grenoble, France, https://orcid.org/0000-0001-6362-0694 (PG); 3. Institute of Earth Sciences, Academia Sinica, Taipei, Taiwan, https://orcid.org/0000-0003-4374-4256 (C-JL); https://orcid.org/0000-0002-1039-6833 (C-SK); https://orcid.org/0000-0003-4905-1960 (B-SH)

*Corresponding author: katepili@gmail.com

Cite this article as Chen, Y., P. Guéguen, K. H. Chen, C.-J. Lin, C.-S. Ku, W.-G. Huang, B.-S. Huang, and K.-C. Chen (2023). Dynamic Characteristics of TAIPEI 101 Skyscraper from Rotational and Translation Seismometers, *Bull. Seismol. Soc. Am.* **XX**, 1–20, doi: 10.1785/0120220147

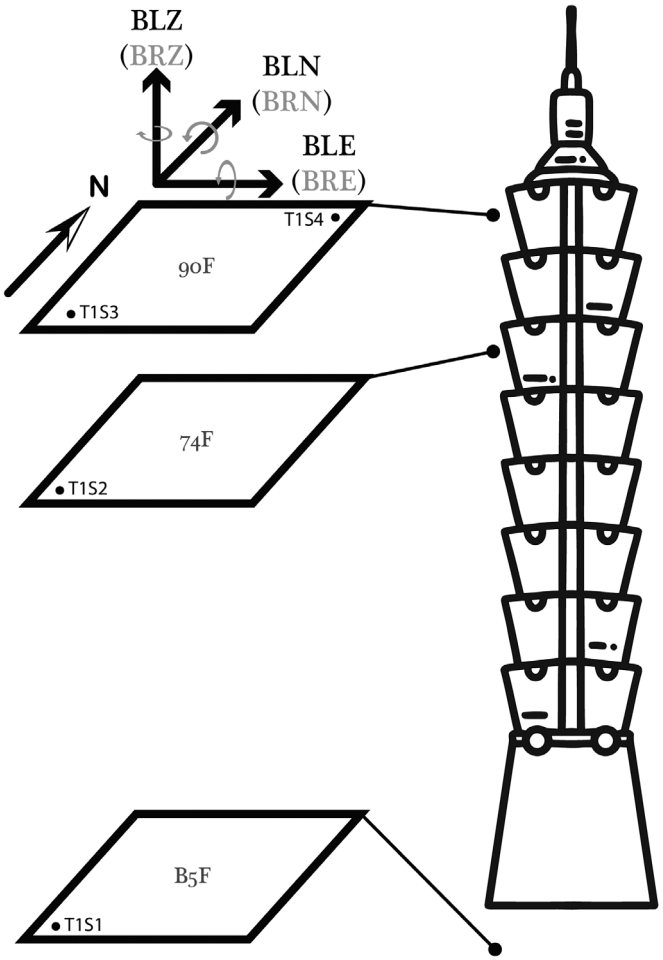

Figure 1. Location of seismometers in TAIPEI 101. The seismometers were installed on the B5th (T1S1), 74th (T1S2), and 90th (T1S3 and T1S4) floors. Their locations on a given floor are denoted by black circles. Note that only the seismometers on the 90th floor recorded rotational velocity data and horizontal acceleration at the same time. The seismometers on the other floors only record acceleration and strong motion.

(e.g., Clinton *et al.*, 2006; Chen *et al.*, 2012; Astorga *et al.*, 2018) and (2) quasi-static changes caused by atmospheric loading such as air temperature and wind (e.g., Mikael *et al.*, 2013; Guéguen *et al.*, 2016; Mordret *et al.*, 2017). Recent full-scale observations in real buildings related to nonlinear elasticity (Guéguen *et al.*, 2016), slow dynamics (Guéguen *et al.*, 2016; Astorga *et al.*, 2019), and fluctuation-dissipation processes (Brossault *et al.*, 2018) have also been reported, advancing the data-driven science behind structural health assessment and seismic response prediction.

Rapid global urbanization has required improved technologies and practices for the long-term monitoring of high-rise buildings as well as seismic fragility and vulnerability models that depend on their condition. The design of high-rise buildings is mainly determined by wind loads (e.g., Tuan and Shang, 2014), the mass of the building, damper design, and internal structure. TAIPEI 101, designed to be generally flexible to handle strong winds but stiff enough to reduce sway and discomfort for occupants, is an emblematic skyscraper. Recognized as the tallest building in the world from 2004 to 2010, TAIPEI 101 is located in Taiwan, an earthquake- and typhoon-prone region. It was constructed in 2004 with 101 floors (590 m high) and five additional basement levels (reaching 19.4 m below the surface). The tower corners are sawtooth shaped above the 25th floor (25F), the super columns are filled with high-strength concrete to improve the stiffness of the system, and the pendulum of the 660 metric ton tuned mass damper (TMD) hangs between the 88th and 92nd floors with a swing rate calculated to overcome the impact of extreme events that induce significant vibration in the building. A full description of the building design can be found in Li *et al.* (2011).

In 2010, the Institute of Earth Sciences, Academia Sinica, Taiwan, deployed four permanent seismic stations in TAIPEI 101. As shown in Figure 1, to monitor the tower response to wind and earthquakes, one permanent station was deployed on the fifth floor below the ground (B5F) and the 74th floor (74F), and two were deployed on the 90th floor (90F), both of which had translational and rotational sensors. The translational components are referred to as BLZ, BLN, and BLE (together abbreviated as BLx) representing the vertical, north–south, and east–west components, respectively, whereas rotational components are referred to as BRE, BRN, and BRZ (abbreviated as BRx) as denoted in Figure 1. The modal characteristics of the tower have been investigated under typhoon and earthquake loading by temporary experiments (Li *et al.*, 2011) and the permanent network (Chen *et al.*, 2012). The natural frequencies of TAIPEI 101 was found to be 0.15 Hz in translation (bending mode) and 0.24 Hz in rotation (torsion mode). The long-period response (<1 Hz) of such tall buildings brings into question their seismic capacity regarding strong, distant earthquakes, such as the 2008 M_w 8 Sichuan earthquake in China (epicentral distance, 1900 km) (Li *et al.*, 2011) and the 2011 M_w 9.1 Tohoku earthquake in Japan (epicentral distance, 2000 km) (Chen *et al.*, 2012). Nevertheless, there exist essential issues to be addressed regarding the response of TAIPEI 101 to ambient vibrations and the natural wandering of its modal parameters with regard to the monitoring of its structural health and seismic response.

Here, we use one-year of continuous translational and rotational seismic data recorded in 2014 to assess the characteristics of the natural frequency of TAIPEI 101. We first describe the building array of TAIPEI 101 and the waveforms from the translational and rotational seismometers on 90F (see the Data section). The methods used to determine the modal frequencies are then introduced in the Determination of modal frequency section. In the Long-term ambient building vibration section, we establish how the modal frequencies change with weather conditions and vibration amplitude. In the

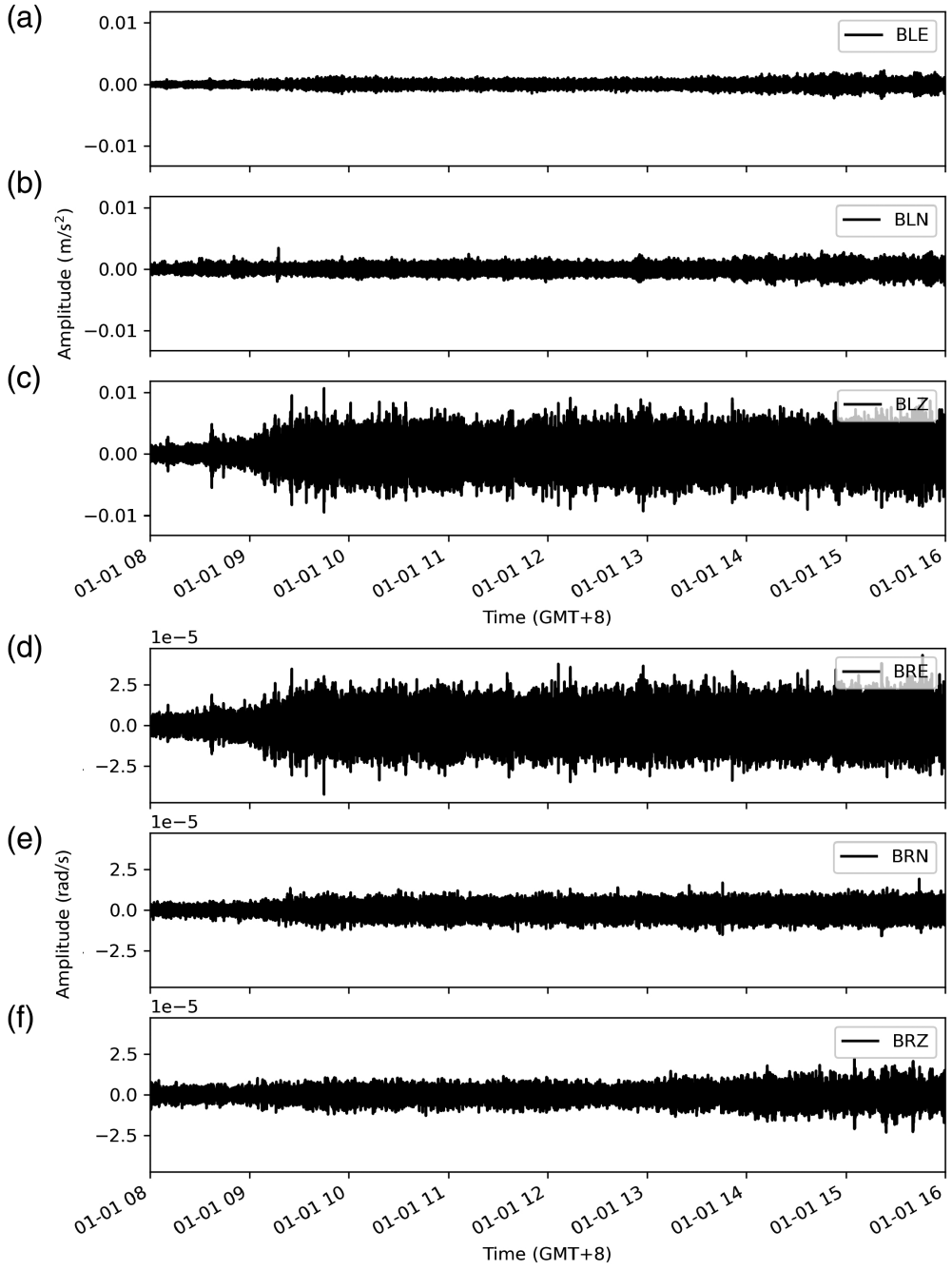

Figure 2. Waveforms for all six components at the southwestern site on 90F (T1S3). Here, the waveforms were detrended with the mean and instrument response removed. (a–c) Display the waveforms for the three translational components BLx, and (d–f) the three rotational components BRx.

Short-term wandering of vibration section, we focus on the hourly variation to explore the possible controlling factors for the short-term variation of modal frequencies. In the Discussion and Conclusions section, we summarize the remarkable features observed in TAIPEI 101, including different characteristics of translation versus rotation, first versus higher modes, and long- versus short-term variation, and then discuss the possible mechanisms.

DATA

Seismic data

The instruments installed on B5F, 74F, and 90F use the six-channel 24-bit Kinemetrics Basalt digitizers. Four stations —T1S1, T1S2, T1S3, and T1S4 —are located at the southwestern corner on B5F, 74F, 90F, and the northeastern corner of 90F, respectively (Chen *et al.*, 2012). Both sites on 90F (T1S3 and T1S4) are also equipped with one three-axis rotational sensor (Eentec R-1). In this study, the data recorded at T1S3, which consisted of both translational acceleration (m/s^2) and rotational rate (rad/s), were considered in exploring the one-year building response under ambient vibration (Fig. 1). The continuous data used here are sampled at 20 Hz. Examples of BLx and BRx waveforms at T1S3 (southwest corner of TAIPEI 101) from 8 to 16 January 2014 (GMT + 8) are shown in Figure 2. The BLx components reveal a larger amplitude in the vertical direction (Fig. 2c), whereas the BRx components show the largest amplitude is in the east–west direction (Fig. 2d). In BRE component, 214 days from the 2014 study period are incomplete because of the missing data points in the daily continuous data. Because of such discontinuity of the data, BRE is considered problematic and thus was not used in the following analysis.

Meteorological data

The 2014 meteorological data collected from weather stations were also used to investigate their relationship with the TAIPEI 101 seismic data. The Central Weather Bureau (CWB) Xinyi station is located only 1.06 km from TAIPEI 101. The recordings of precipitation, air pressure, relative humidity, temperature, wind velocity, and wind direction were processed using a

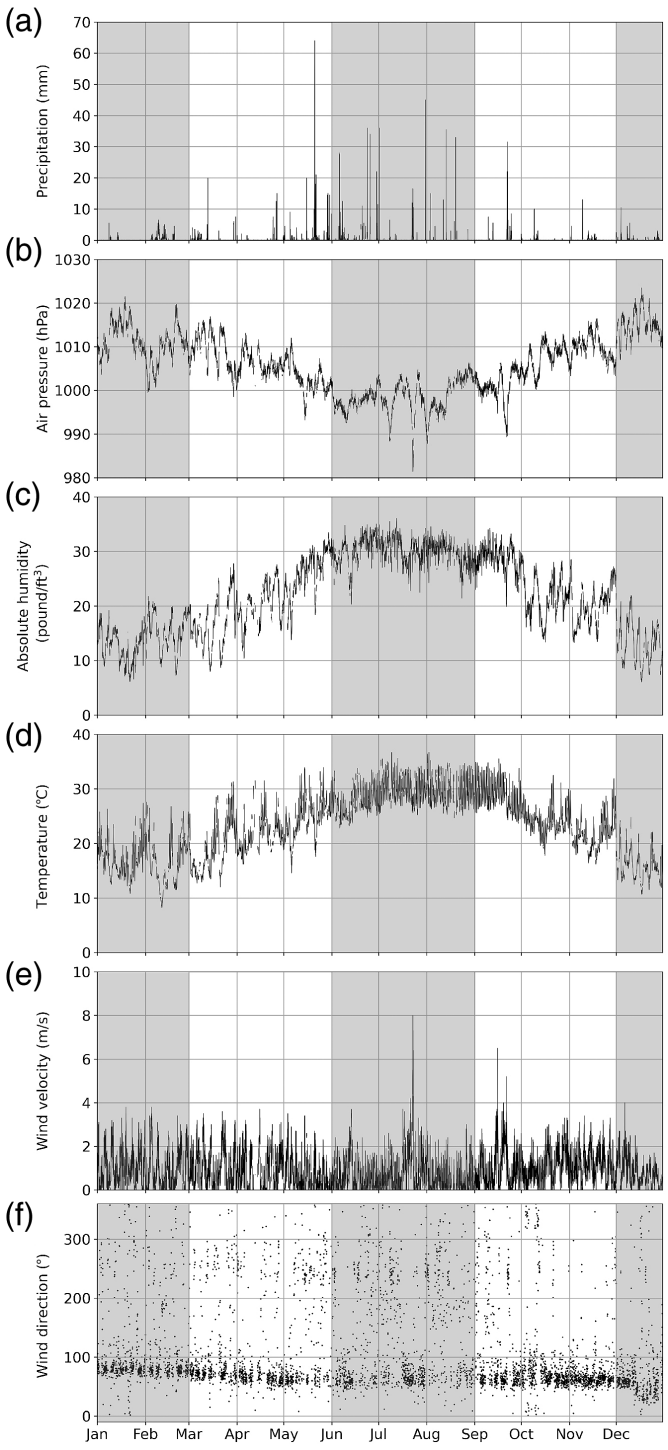

Figure 3. Continuous weather data recorded at the nearby Central Weather Bureau (CWB) Xinyi station (25.0396° N, 121.5564° E) in 2014 with hourly sampling rate. (a–f) The continuous recordings for precipitation, air pressure, absolute humidity, temperature, wind velocity, and wind direction, respectively. The gray areas indicate the summer and winter seasons in Taiwan.

1 hr sampling rate and are displayed in Figure 3. The absolute humidity (H_{abs}) can be obtained using the recorded relative humidity (H_{rel}) as follows:

$$e_s(T) = 6.112 \exp\left(\frac{1.67T}{T + 243.5}\right), \tag{1}$$

$$H_{abs} = H_{rel} \times e_s(T), \tag{2}$$

in which T and e_s represent air temperature (°C) and vapor pressure (mb), respectively. As shown in Figure 3, the heavier precipitation during June–August coincides with lower air pressure, higher absolute humidity, and higher temperature. The wind velocity and direction, however, do not reveal significant seasonality. The occasionally large wind velocities tend to occur in August and October because of the typhoons that occurred during the periods of 14–15 June (Hagibis, light typhoon), 21–23 July (Matmo, medium typhoon), and 19–22 September (Fung-Wong, light typhoon). Using 2010–2012 meteorological data from the CWB weather station (Xinyi site station) located within the basin and close to TAIPEI 101, Lai (2018) showed that during the day the most prominent wind direction was between 33.75° and 101.25° (easterly wind), mainly from the sea. At night, the wind direction was between 101.25° and 168.75° (southerly wind), mainly from inland. In Figure 3f, the wind direction appears to concentrate around 90°, which is easterly wind likely caused by the sea and land breezes interacting with changes in the local topography. There exists a large amount of zero wind direction in Figure 3f. The reason is that wind direction is recorded as zero when the wind velocity is under the detection limit (0.2 m/s). Thus, in the following analysis, wind velocity <0.2 m/s is excluded. As shown by the scatter plots in Figure 4, the temperature appears to be linearly related to humidity and air pressure, indicating a strong dependency between these three parameters. The high wind velocity and precipitation, however, are mainly controlled by extreme events and do not show clear correlations with the other parameters. This can also be seen in Figure S1, available in the supplemental material to this article.

DETERMINATION OF MODAL FREQUENCY

Random decrement technique

The ambient vibration recorded in a building generally contains random and stationary signals that contain the impulse response of the structure. If a building is considered to be a linear single-degree-of-freedom (SDOF) system, the response of the building can be expressed as follows:

$$v''(t) + 2\zeta\omega v'(t) + \omega v(t) = -v_g'', \tag{3}$$

in which ω and ζ represent the specific angular frequency and the damping ratio, respectively, and v_g'' represents the loading. After a selected time window, $v(t)$ can be further separated into the forced (stochastic) and the free (deterministic) responses of the system as $v_1(t)$ and $v_2(t)$, respectively. Each segment can be considered as the sum of two mathematical expectations of $v_1(t)$

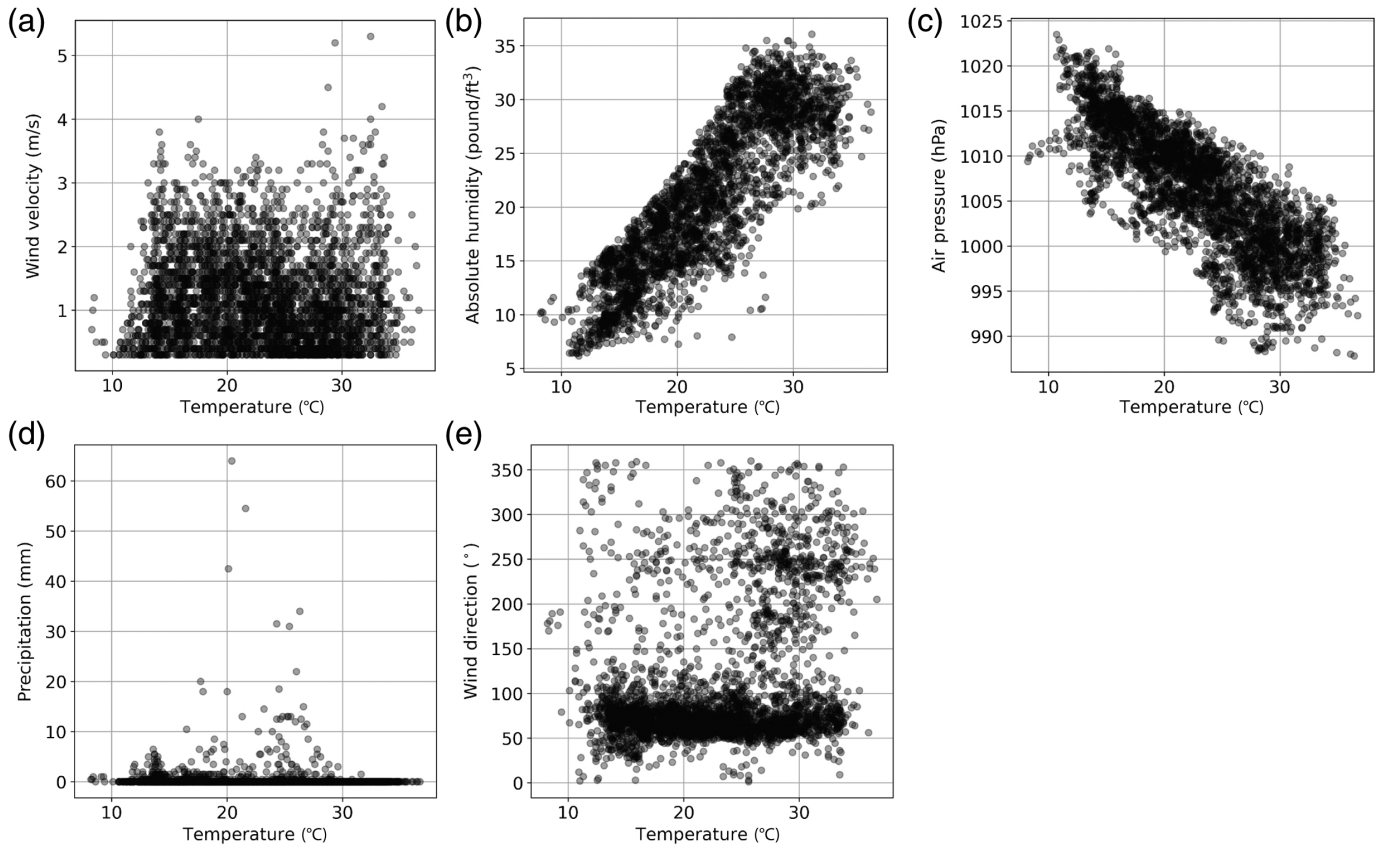

Figure 4. Scatter plots of (a) wind velocity, (b) absolute humidity, (c) air pressure, (d) precipitation, and (e) wind direction versus temperature. The data were recorded at XinYi station, 1.06 km away from TAIPEI 101 with hourly sampling rate.

as constant and $v_2(t)$ as the free response of the SDOF, assuming an ergodic process. The random decrement technique (RDT) (Cole, 1968) is the averaged triggered time window of the signal recorded at the top of the building leading to the random decrement signature (RDS) subsequently:

$$\mathrm{RDS}(\tau) = \frac{1}{N}\sum_{i=1}^{N} s(t_i + \tau). \tag{4}$$

Here, τ is the duration of each $s(t)$ signal window. In practice, by stacking and averaging sufficient segments with the same initial conditions, the coherent signals converge toward the impulse response of the structure, which decreases exponentially in the form of $e^{-\zeta\omega t}$. By fitting an exponential decay, the circular frequency ω and damping ratio ξ can be obtained. In this article, only resonant frequencies are addressed.

To obtain a stable and reliable damping ratio, it is crucial to use a sufficient number of segments (N) in RDS. Jeary (1997) stated that at least 500 windows are needed to obtain a robust measure of RDS. In this study, the 1 yr data record was prepared and segmented into 1 hr long signals that are equivalent to or more than 1000 periods (considering that the resonance frequency of TAIPEI 101 is <1 Hz). To refine the impulse responses of TAIPEI 101 in bending and torsion modes using RDT, a filter scheme was predetermined based on power spectral density (PSD) plots obtained for six different components. For hourly data, multiple signal windows that contained eight cycles were prepared, band-pass filtered within a bandwidth of ±0.02 Hz of the center frequency determined by the peaks in PSD.

PSD

The PSD plots are shown in Figure 5. The greater amplitude in BRE and BLZ appears to be a contribution from the higher than 5 Hz energy, which is likely associated with anthropogenic processes as explored by Chen *et al.* (2022), for which the 2–10 Hz energy concentrations are interpreted as city traffic induced vibrations. In rotation, the torsion modes (rotation around the vertical axis, BRZ) denoted by R1, R2, and R3 in Figure 5f correspond to 0.23 Hz, 0.59 Hz, and 0.93 Hz for the fundamental, first, and second modes, respectively. The R1 can also be observed in the translational (horizontal) PSD as noted in Figure 5a–e. In translation (BLE and BLN), the fundamental and higher modes of resonance (F1–F3 in Fig. 5) are 0.15 Hz, 0.43 Hz, and 0.78 Hz, respectively, following the classical series of frequencies for a pure shear beam-like building (3, 5, 7, and so on). Rotations around the horizontal direction (BRE and BRN) have the same frequencies as a result of the coupling

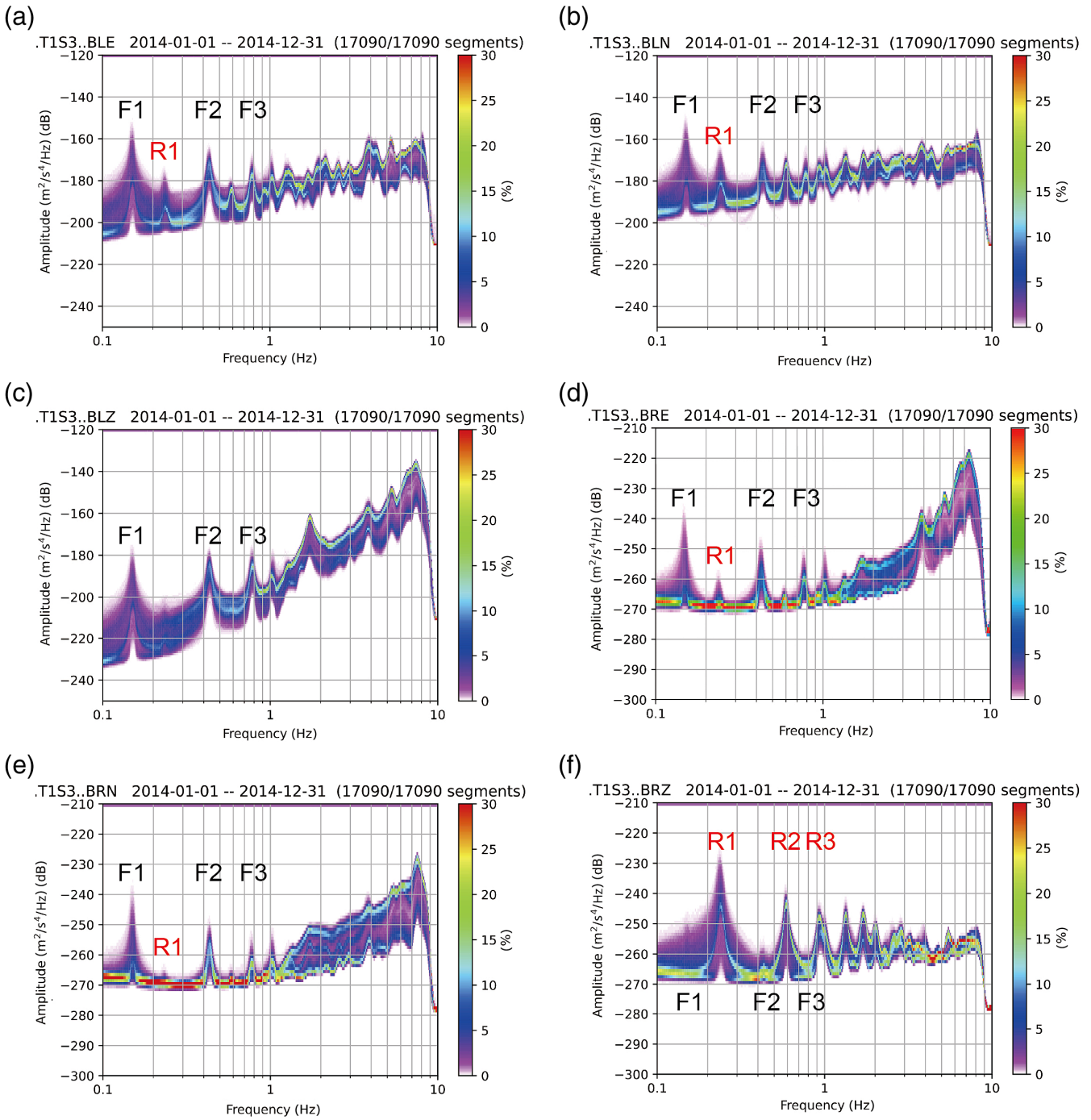

Figure 5. Power spectral density (PSD) plots of all components on 90F. (a–c) PSDs of the horizontal components and (d–f) PSDs of the rotational components. Note that each spectrum represents 1 hr of data without overlap over the year of 2014. The color version of this figure is available only in the electronic edition.

between the translation and rocking motion of such a tall building. In both symmetric and asymmetric buildings, the input loading in both horizontal directions may modify the dynamic response of the structure through the coupling of the translational and rotational modes of vibration (Douglas and Trabert, 1973). For further comparisons of rotation and translation, please refer to the review article by Guéguen and Astorga (2021).

The long-term variation frequencies and damping were computed hourly using RDT. As shown in Table 1, the average modal frequencies (F1–F3), the damping ratio, and their coefficient of variance (COV) are listed for different components. The frequency appears to show slightly larger variation in F1 for all components, as indicated by an ~2–10 times larger COV compared with that of F2 and F3. A much greater degree

TABLE 1
Modal Frequency and Damping Ratio of F1–F3 and R1–R3 for Each Component

Component	Mode	Frequency (Hz)	COV_F	Damping (%)	COV_D
BLE	F1	0.151	0.0046	0.470	1.1214
	F2	0.434	0.0021	0.339	0.2478
	F3	0.782	0.0012	0.138	0.2097
BLN	F1	0.149	0.0095	0.893	1.4090
	F2	0.428	0.0024	0.437	0.2992
	F3	0.774	0.0016	0.233	0.2104
BLZ	F1	0.151	0.0037	0.532	0.5638
	F2	0.434	0.0023	0.397	0.2409
	F3	0.782	0.0014	0.159	0.1706
BRE	F1	0.147	0.0396	2.089	1.0515
	F2	0.428	0.0040	0.730	0.9384
	F3	0.775	0.0036	0.280	0.3926
BRN	F1	0.150	0.0285	2.050	1.0586
	F2	0.434	0.0021	0.427	0.2891
	F3	0.778	0.0018	0.292	0.1497
BRZ	R1	0.234	0.0070	1.413	0.3657
	R2	0.590	0.0027	0.217	0.2045
	R3	0.928	0.0025	0.170	0.1398

COV, coefficient of variance.

of scattering of the measurements, however, is observed for the damping. The COV is >1.0 in F1 for most of the components except for BRZ, suggesting that the damping is much more influenced by the natural wandering of the building response. Because of the complexity of the damping variation, we only focused on modal frequencies in the current study.

By subtracting the averaged value, the centered frequency can be calculated from

$$F_{\text{cent}} = F - F_{\text{avg}}, \tag{5}$$

in which F represents the daily measurements and F_{avg} represents the annual average obtained from RDT. Figure 6 shows the temporal variation of the frequency over one year for different components. Daily resolution was applied to establish the long-term behavior because the 1-yr data were segmented into 1-day signals and averaged instead of the 1-hr signals considered in RDT and PSD. In general, the BLx components and BRZ reveal less variation in their centered frequency across different modes, corresponding to the smaller COV shown in Table 1. During summer, a relatively high frequency is seen in many components except for BRZ, suggesting that the rotational motion of the building may respond differently to the seasonal environmental factors (e.g., air temperature and air pressure). In fact, changes in meteorological conditions have been found to produce a softening effect on building vibration, leading to an alteration in modal frequencies, damping ratios, and amplitudes (Clinton *et al.*, 2006; Stehly *et al.*, 2006; Herak and Herak, 2010; Hillers *et al.*, 2012; Guéguen *et al.*, 2016). In the following section, we establish to what degree the meteorological conditions and vibration amplitude modulate the bending and torsion modes of TAIPEI 101.

LONG-TERM AMBIENT BUILDING VIBRATION

During earthquakes, the modal frequency of a building can change dramatically because of structural damage. Under ambient conditions, small changes in the natural frequency can also occur. It is known from theoretical and experimental studies that the ambient vibration of a building is sensitive to changes in the boundary conditions and the mechanical and elastic properties of the material (e.g., Jennings and Kuroiwa, 1968; Crouse and Jennings, 1975; Todorovska and Trifunac, 2007; Todorovska, 2009). The nonlinear responses of a building also play a role, such as in the transient variations caused by a nonlinear response of the soil-structure boundary during seismic excitation or because of the closing and opening processes of preexisting cracks within the buildings (e.g., Luco *et al.*, 1987; Meli *et al.*, 1998; Clinton *et al.*, 2006; Michel and Guéguen, 2010). It is known from observational studies that fluctuations in the fundamental frequency of a building often correlate with temporal variations in the meteorological conditions and vibration amplitude (Song *et al.*, 2019; Martakis *et al.*, 2022).

Compared with earthquake-induced shaking that only lasts a few minutes, the response of high-rise buildings to quasi-dynamic forcing under meteorological conditions has been less explored because of a lack of a continuous and permanent monitoring system. Experiments involving vertical clamp-free beams and observations of buildings in France and the United States have demonstrated that the frequency and damping ratio are related to air temperature (Brossault *et al.*, 2018). Factors that affect the diffusion of heat in a building and thus control its temperature (e.g., the type of cladding used in construction, which side of the building faces the sun, and differing foundation conditions) have been identified as physical mechanisms underlying the frequency changes with temperature (e.g., Clinton *et al.*, 2006; Hua *et al.*, 2007; Nayeri *et al.*, 2008; Mikael *et al.*, 2013).

To explore the first-order factors that influence the continuous bending and torsion modes of TAIPEI 101, we next detail the meteorological parameters (i.e., precipitation, air pressure, absolute humidity, air temperature, wind velocity, and wind direction) recorded at the nearby weather station, Xinyi, and their association with the observed frequency behavior. The original weather data and modal frequencies computed by RDT are characterized by the sampling rate of one hour. However, to avoid the large variation of modal frequencies in a day, the seasonal change of modal frequencies is computed and plotted by daily average. Therefore, in the demonstration of their temporal distribution, the weather data are plotted by hourly resolution to emphasize the extreme events, whereas the modal frequencies are plotted by the daily average in the following analyses.

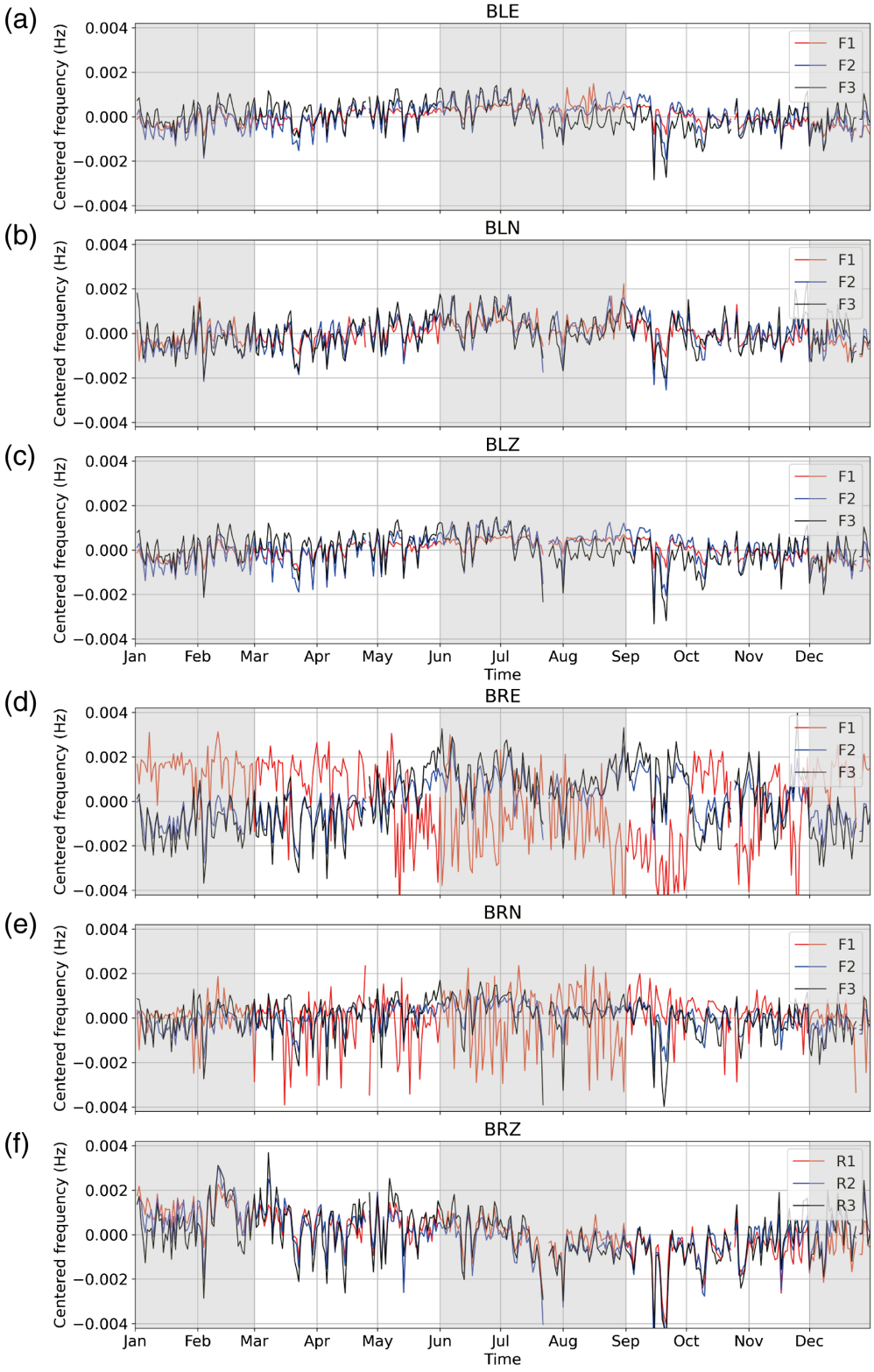

Figure 6. Temporal variation of the centered frequency for all components. (a–c) The centered frequency of all modes for BLE, BLN, and BLZ. (d–f) The centered frequency of all modes for BRE, BRN, and BRZ. The result of the one-day-average of F1–F3 (or R1–R3) are shown by the red, blue, and black solid curves, respectively. Here, the original modal frequencies computed by hourly data is smoothed by daily average to avoid the large variation in a day. To be comparable with different components, the absolute frequency is computed by subtracting the averaged value as "centered frequency" here. The color version of this figure is available only in the electronic edition.

Influence of meteorological conditions

The dependency of modal frequency on six environmental factors is demonstrated in Figure 7 for BLE and BRZ as examples. The median value of the observations in each bin is represented by black circles, and the standard deviation is indicated by the length of the vertical black line (Fig. 7). Here, the bin width corresponds to 10% of the total range of the observations (e.g., for the temperature range of 7°C–17°C, the bin size was selected as 1°C). If the data points in each bin were <5% of the total number of observations (365 for one year), the average and standard deviation were discarded. In Figure 7, the first mode of the BLE component reveals that the frequency decreases with increasing air pressure and wind velocity (Fig. 7b,e) but increases with increasing absolute humidity and air temperature (Fig. 7c,d). The precipitation and wind direction data points are more concentrated with a small range of observations, and thus no clear trend is evident (Fig. 7a,f). A similar trend is also observed in rotational motion (Fig. 7g–l). In general, the frequency has a clear trend with the change in air pressure, absolute humidity, temperature, and wind velocity. The points in the diagrams of frequency versus precipitation and wind direction, however, are scattered without any clear trend. Temperature and wind velocity are thus regarded as the key parameters that determine the primary frequency of the building. For the first mode of the BRZ component (R1), however, the relationship

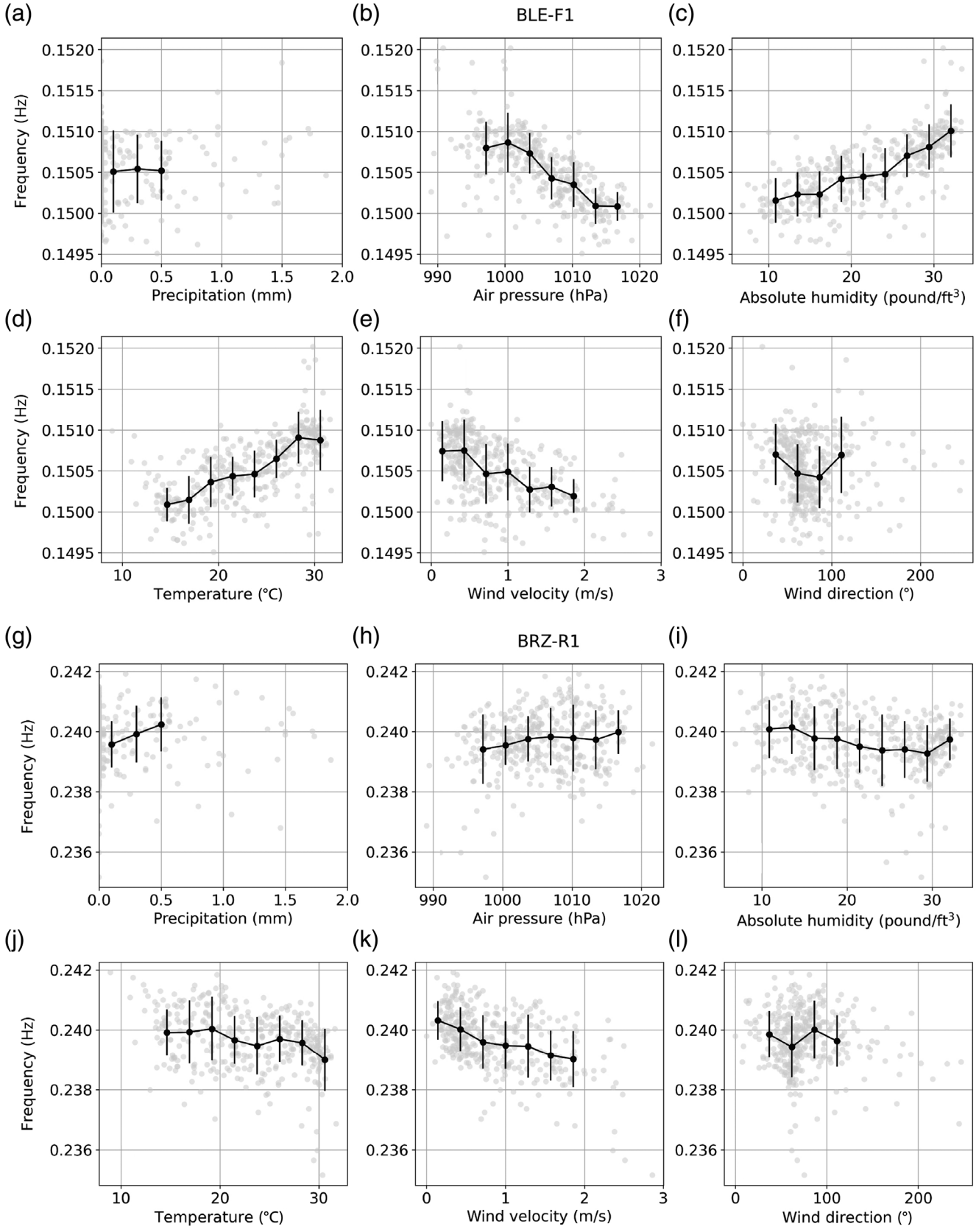

Figure 7. Scatter plots of frequency and environmental factors of (a–f) F1 for BLE and (g–l) R1 for BRZ. Plots (a–f) and (g–l) show the frequency dependence on precipitation, air pressure, absolute humidity, temperature, wind velocity, and wind direction. The light gray dots show the daily average frequency of F1 for BLE and R1 for BLZ. The black solid lines show the mean and standard deviation of frequency in each 10% variance bin for the different environmental factors. Here, the absolute frequencies are obtained from the one-year of data using a daily sampling rate.

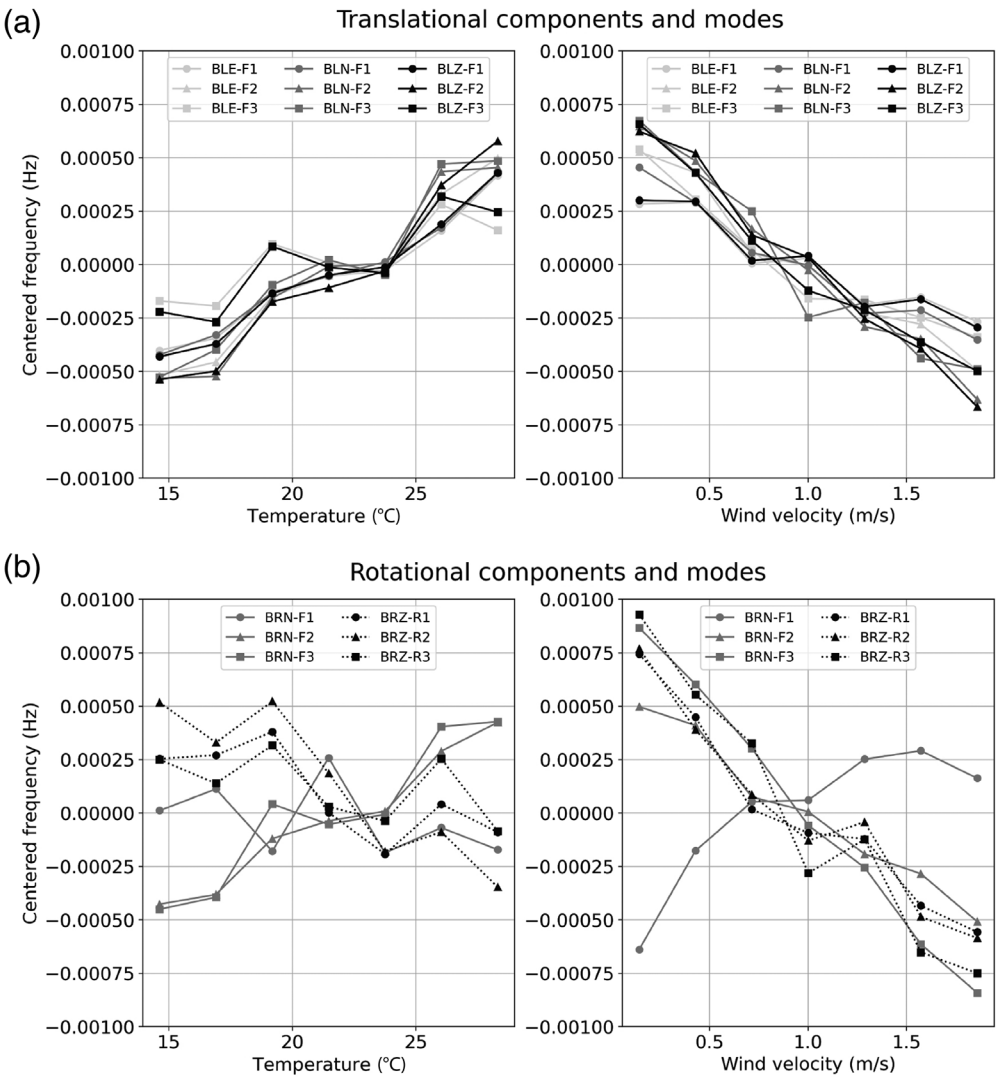

Figure 8. Dependency of frequencies on meteorological conditions for different modes for (a) translational components (BLx) and (b) rotational components (BRx). The BRE component was discarded because of the discontinuity of the data. Different symbols represent different modes. (a–b) Dependency of frequency on temperature and wind velocity of F1–F3/R1–R3 for horizontal and rotational components, respectively. Note that the absolute frequency in Figure 7 is now used to subtract the averaged value here as the centered frequency to provide a better comparison between different modes.

between the frequency and air pressure, absolute humidity, and temperature seems to be reversed (Fig. 7h–j), but the trend for wind velocity remains the same (Fig. 7k). The difference in frequency dependence on temperature, air pressure, and absolute humidity in rotational motion are interconnected as revealed in Figure 4, in which increasing temperature corresponds to increasing absolute humidity and decreasing air pressure. We found that the reverse trends between Figure 7c,d and Figure 7i,j are mainly attributable to the different temperature dependency on frequency for F1 and R1.

The same presentation for higher modes and other components can be seen in Figure 8. To simplify the trends to allow for a better comparison of the different modes, at least 36 data points were required for each bin to obtain the median values. For the translational components (Fig. 8a), F1–F3 reveal very similar trends, indicating a common dependency of frequency on temperature and wind velocity. In the rotational components, however, the modal frequencies display more complicated behavior, especially with respect to temperature (Fig. 8b). The centered frequencies show a strong dependency on wind velocity except for F1 for BRN. On the other hand, in rotational motion, the frequency versus temperature plot displays more scattered trends and a weaker dependency on temperature. For BRN, the centered frequency appears to increase with increasing temperature; for BRZ, the trend is reversed. In general, the higher modes in both translational and rotational motions appear to behave similarly (Fig. 8). It is clear that the temperature has a different impact on the modal frequencies for translation and rotation. The different frequency versus temperature behavior for rotational motion suggests the importance of introducing rotational motion analysis into structural health monitoring. The possible mechanisms is discussed later in the Dependency of natural frequencies on temperature in rotational motion section.

The correlation between modal frequencies, temperature, and wind velocity can be established by their temporal distribution. The temporal variation of the fundamental frequencies recorded on 90F over the year for the different components are compared with temperature and wind velocity in Figure 9. Each measurement was divided by the averaged value and multiplied by different factors to make them easier to compare and line up within the same figure. A clear seasonal trend is seen in temperature (red) but not wind velocity (black) recorded at the weather station on the ground. In translational motion (orange, blue, and green), the fundamental frequencies

Figure 9. Temporal variation of temperature, wind velocity, and fundamental frequency for different components. BRN and BRZ components are denoted by pink and light-blue lines, whereas BLZ, BLN, and BLE components are denoted by yellow, blue, and green lines, respectively. The temperature and wind velocity recorded at the weather station on the ground are denoted by red and black lines. The wind velocity recorded in TAIPEI 101 is indicated by dark purple line. Note that there exists missing data points in wind velocity recorded in TAIPEI 101 (purple) during the period of September to mid-November and December. The color version of this figure is available only in the electronic edition.

appear to be very sensitive to temperature. During the hot weather from June to September, the fundamental frequencies are slightly higher. For rotational motion, however, the sensitivity to temperature is less obvious, but F1 shows a stronger correlation with TMD amplitude. As shown in Figure S2, the sudden drop in the centered frequency for BRN F1 appears to correspond to the greater amplitude recorded at the TMD. However, when the TMD swayed more severely from mid-May to late-September, the correlation with the BRN frequency seemed to disappear. This could be associated with the coupling of temperature and TMD vibration. Given that strong winds did not arrive until August, the possible modulation of the elevation of TMD vibration by the increasing temperature during these months requires further investigation and is discussed in the Dependency of natural frequencies on temperature in rotational motion section.

Figure 9 also displays the similarity of the wind velocity recorded at ground and on 90F of TAIPEI 101. As revealed by the dark purple and black curves, the temporal variation of the wind velocity is nearly identical, but the wind velocity recorded on 90F is 2–3 times faster than on the ground. A close-up in January and July can be illustrated in Figure S3, for which a very large peak corresponding to the typhoon Matmo in July is obvious. Even though the wind gust cannot be seen with 1-hr sampling rate, the hourly mean value still reflects the sharp increase in wind velocity. The wind velocity in January tends to show a 5- to 7-day recurrent pattern with a relatively greater magnitude than that in July (Fig. S3c,d). Unlike temperature, which is always highest in summer, the wind velocity is usually faster during winter because the northeast winter monsoon from the Eurasian continent arrives at Taipei more efficiently (because of the short distance) compared with the southwestern summer monsoon from South Asia.

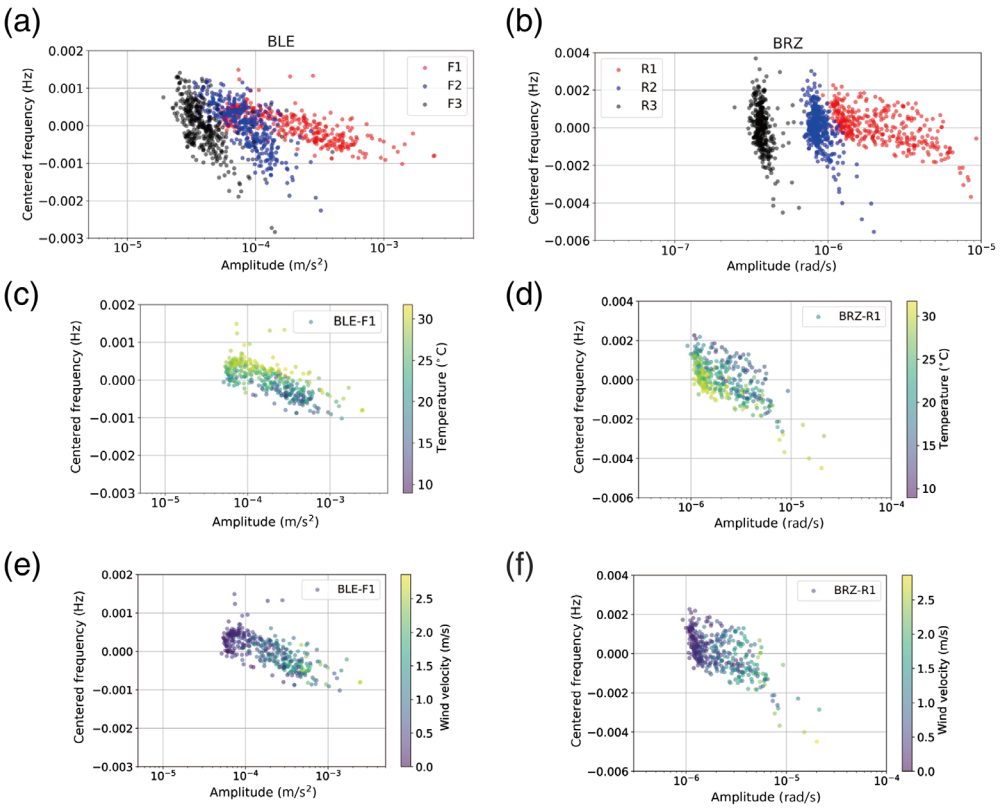

Figure 10. Scatter plot of centered frequency versus amplitude for three different modes with daily sampling rate: (a) the BLE component and (b) the BRZ component. Red, blue, and black circles represent F1, F2, and F3 in (a) and R1, R2, R3 in (b). (c,d) Plots of the relationship between the centered frequency and absolute amplitude for F1/R1, color coded by temperature. (e,f) Plots of the relationship between the centered frequency and absolute amplitude for F1/R1, color coded by wind velocity. The color version of this figure is available only in the electronic edition.

Amplitude dependence of modal frequency

The impact of external loading on the modal frequency of a building has been intensively studied. The decrease in the natural frequency with increasing acceleration amplitude has been widely observed under strong winds (e.g., Fu *et al.*, 2008; Au *et al.*, 2012; He and Li, 2014). It is commonly found that when the vibration amplitude increases, the modal frequency tends to decrease under ambient wind conditions (Tamura and Suganuma, 1996). Jeary (1986) provided an explanation involving the mobilization of larger and more abundant cracks with increasing excitation amplitude. Assuming a constant mass, the opening of the discontinuities will cause a change of the stiffness, which impacts the modal frequency. This is also evident for TAIPEI 101. Li *et al.* (2011) investigated the response of TAIPEI 101 caused by three typhoons and one earthquake and proposed that when the vibration amplitude increases, the natural frequencies decreases, and the damping ratio increases. Using one-year continuous data in this study, the trend of frequency changing with shaking amplitude is well established, which reveals the centered frequency decreasing logarithmically with the amplitude of the motion. As shown in Figure 10a,b, the BLE and BRZ components were chosen as examples to establish the relationship between the centered frequencies and amplitude. Compared with the higher modes (F2 and F3), the primary frequency (F1) has a weaker dependency on the amplitude in both translation and rotation. Other components also show the same tendency toward a weaker dependency in F1 (Fig. S4). This implies that when the vibration amplitude increases under atmospheric or seismic forcings, the corresponding change in the structural properties reflected by modal frequencies for F1 is confined into a much smaller range than predicted by higher modes. Or when the frequency decreases because of to the change in structural stiffness, the corresponding elevation amplitude for F1 is at a lower level than predicted by higher modes.

The possible mechanisms could be anything that generate a less favorable condition for the primary frequency to change, which include the change of the opening of the discontinuities in the building caused by wind loadings (e.g., Tamura and Suganuma, 1996; Fu *et al.*, 2008; Michel and Guéguen, 2010; Au *et al.*, 2012; He and Li, 2014), the soil–structure interaction, and elastic properties of the construction materials (e.g., Clinton *et al.*, 2006; Todorovska and Trifunac, 2008; Todorovska, 2009; Michel and Guéguen, 2010). However, whether the aforementioned condition may alter the frequency behavior differently at different modes remains an open question. Here, we argue that the TMD may play an important role in the distinct amplitude response of primary frequency. The design of the TMD in TAIPEI 101 aims to reduce the vibrations of the building, especially under extreme wind loads and seismic forces. It is thus reasonable to predict a confined frequency change (or reduction of amplitude) in the first mode. From a numerical simulation, Tuan and Shang (2014) established that with TMDs, the first mode is split into two modes of 0.173 and 0.222 Hz from the original 0.209 Hz (without TMDs), whereas the second mode remains identical. Because the resonant response of the first mode is altered significantly due to the TMD system,

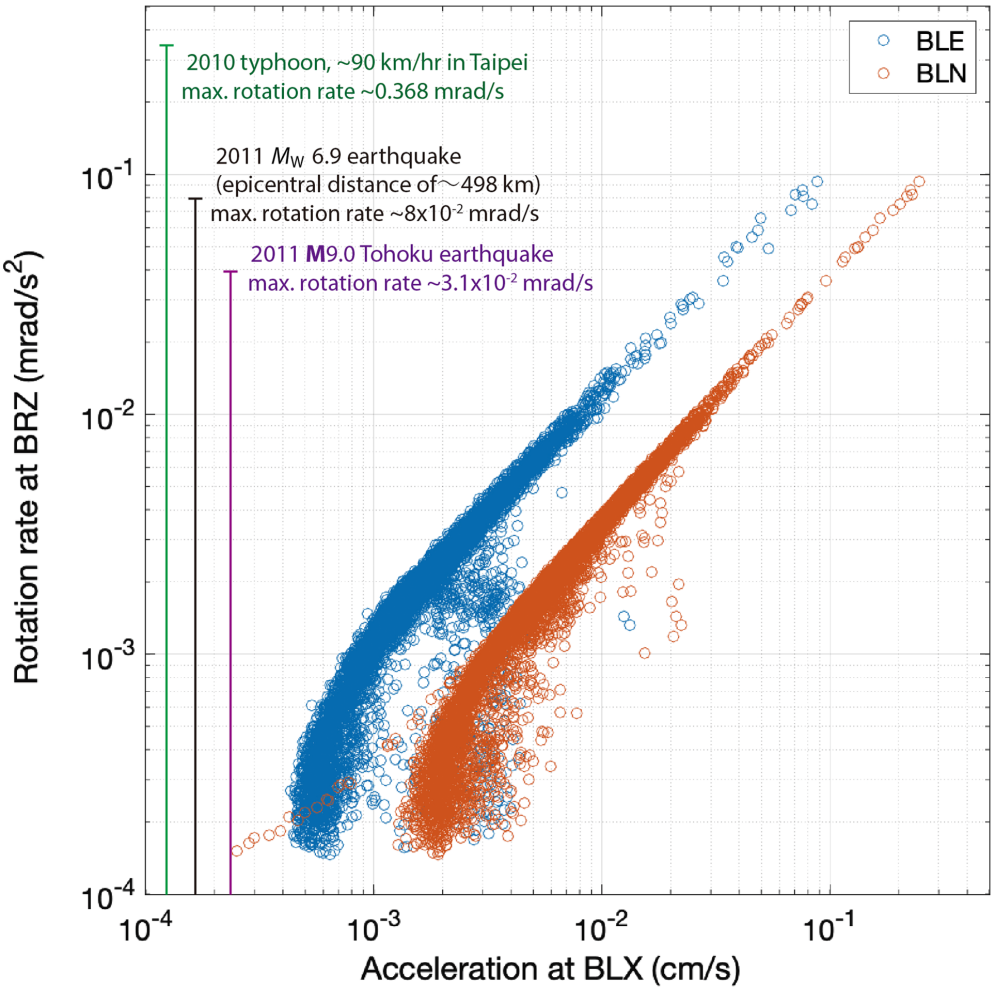

Figure 11. Amplitude correlation between horizontal motion (cm/s^2) recorded at BLE and BLN and rotational motion (mrad/s) recorded at BRZ. Here, the amplitude refers to the absolute value of the hourly median for R1 mode. The orange and blue circles represent data for BLN and BLE, respectively. The maximum rotation rate of 2010 typhoon (green line), 2011 **M** 6.9 earthquake (black line), and 2011 Tohoku earthquake (purple line) was obtained by Chen *et al.* (2013), Lin *et al.* (2012), and Chen *et al.* (2012). The color version of this figure is available only in the electronic edition.

the amplitude of the first mode is suppressed. This probably explains why the dependency of centered frequency on amplitude differs between F1 and F2/F3.

Figure 10c–f reveals the association between amplitude, temperature, and wind velocity. The wind velocity appears to strongly correlate with the absolute amplitude of primary frequencies (Fig. 10e,f) because the amplitude increases with increasing wind velocity. However, the frequency appears to be temperature dependent (Fig. 10c,d). In Figure 10c, in which the BLE data are color coded by temperature, it is evident that higher frequency corresponds to higher temperature. At BRZ, however, a higher frequency corresponds to lower temperature (Fig. 10d). The opposite relationship between frequency and temperature for BLE and BRZ is consistent with the trend seen in Figure 7d,j. This suggests that the temperature effect is likely coupled with the dependence of frequency and amplitude for both translational and rotational responses. Because crack openings have been proposed as causal factors in the dependence of amplitude on the change in stiffness (e.g., Jeary, 1986; Luco *et al.*, 1987; Meli *et al.*, 1998; Michel and Guéguen, 2010) when the dynamics of a crack inside the structure change with temperature, it is reasonable to consider that the effect of temperature is coupled with the frequency versus amplitude relationship.

Correlation between translation and rotation

Because a comparison between translation and rotation may reflect the resistance of the building, we also examined and compared the amplitude for the translational and rotational components. BRZ records the pure rotation, and BLx records the translation that is coupled with torsion; R1 can also be seen in BLE and BLN (see R1 indicated in red in Fig. 5). The variation in frequency with respect to R1 mode (0.234 Hz) for BLE and BRZ is shown in Figure 11. Most of the data fit a linear trend having a 1:1 relationship, and the scattering of data points mostly occurs at values $<10^{-2}$ cm/s^2 (blue circles). The R1 amplitude recorded at BRZ is compared with those recorded for BLE and BLN in Figure S5. As can be seen in Figure 11 when the rotation rate is $>10^{-3}$ mrad/s, there exists a linear relationship between the rotational rate and translational rate with a slope of ~1. When the rotational rate is smaller than 10^{-3} mrad/s, the ratio of the rotational to translational rate increases (>1). The same 1:1 relationship between the peak rotational velocity (<0.1 mrad/s) and peak ground acceleration (<0.3 cm/s^2) has been previously explored in free field using 52 local earthquakes in Taiwan (Liu *et al.*, 2009). Guéguen and Astorga (2021) examined earthquake data and also observed a ratio of 0.716 and 2.818 at the base and top (8F) of the foundations, respectively, whereas the rotational and

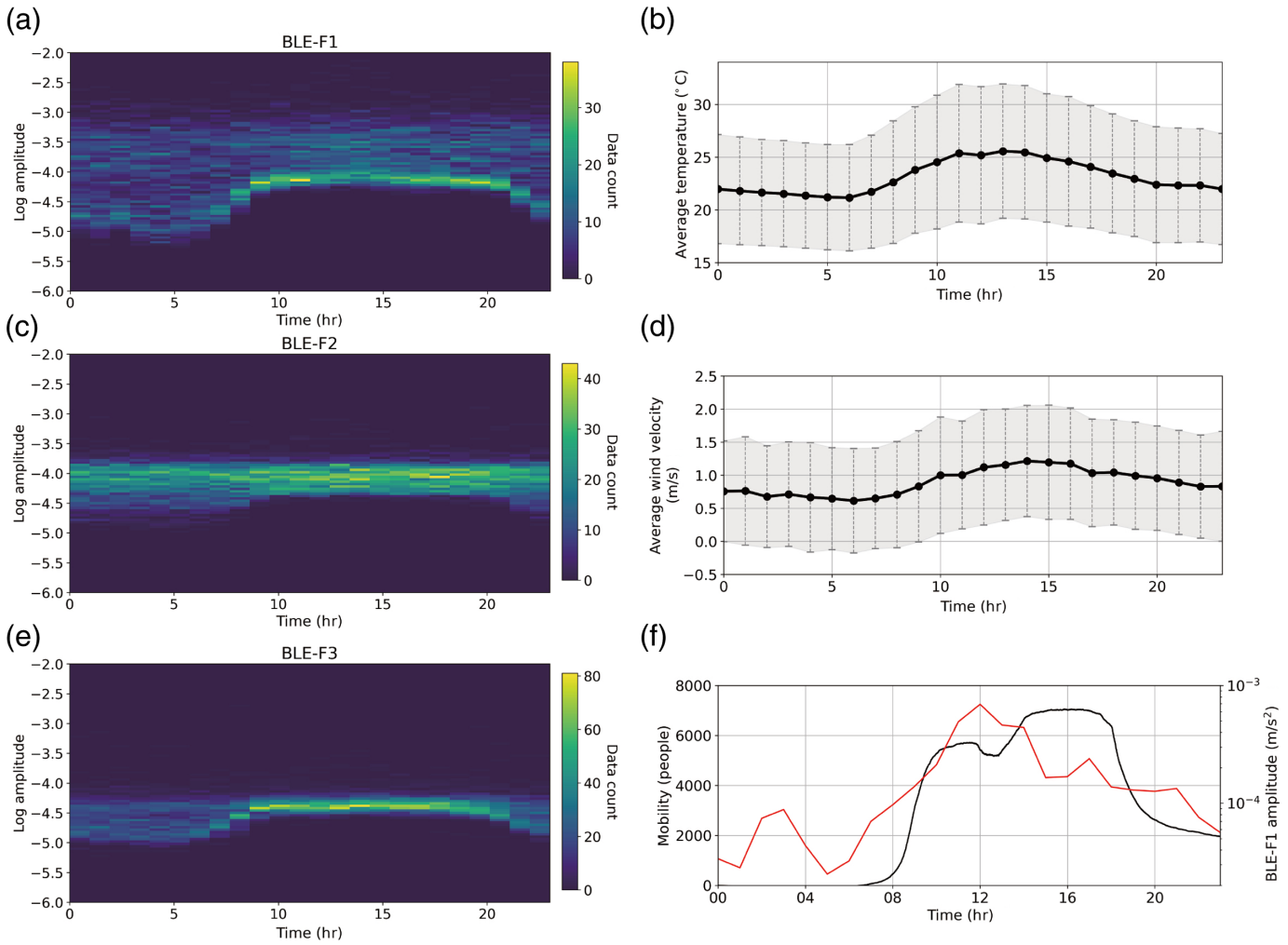

Figure 12. Density plot for hourly variation in amplitude at BLE using one-year-long data for (a) F1, (c), F2, and (e) F3 modes. The temperature and wind velocity computed using the hourly data are shown in (b) and (d), respectively. (f) The amplitude of F1 at BLE (red line) and mobility (black line) in TAIPEI 101 on 6 July 2022. The mobility data provides the number of employees in this business building counted in every entryway for when they entered and exited. Note that this entrance counter does not include the record of tourists and visitors. The color version of this figure is available only in the electronic edition.

translational motion ranged from 10^{-2} to 10^{1} mrad/s and 10^{-1} to 10^{3} m/s^2. Comparing with the rotation rates recorded during the 2011 **M** 9.0 Tohoku earthquake (0.031 mrad/s) and 2011 **M** 6.9 earthquake (0.08 mrad/s) and typhoon Fanapi in 2010 (0.368 mrad/s) (Chen *et al.*, 2012, 2013), we are able to establish a very small motion of 10^{-4} to 10^{-1} mrad/s and 10^{-4} to 3×10^{-1} cm/s^2 in this study. The ambient vibration on 90F of the building exhibits at least 200 times smaller magnitude than the one during typhoon. Special attention should go to the change of rotation rate versus acceleration correlation in Figure 11. The transition occurs at 9×10^{-4} mrad/s, indicating that the relationship between the translation and rotation rate cannot be described by a simple straight line under weak motion of $<7.5 \times 10^{-4}$ cm/s^2 and 9×10^{-4} mrad/s. This encourages the careful treatment to estimate the rotation rate of building response using translation sensors, under very weak motion.

SHORT-TERM WANDERING OF VIBRATION

To observe the vibration of TAIPEI 101 with a finer temporal resolution, we next established the hourly variation of the modal frequencies. The one-year data were stacked into a 24-hr-long window for a display of amplitude variation over time. As shown in the density plots in Figure 12, the number of data points in each grid (1 hr $\times 10^{0.05}$ m/s^2) was counted and color coded. For F1 shown in Figure 12a, the concentration of relatively high amplitudes ($>10^{-5}$ m/s^2) occurred from 9 a.m. to 9 p.m.; from 8 p.m. to 8 a.m. the amplitude was ~10 times smaller. Such stable and long-lasting amplitude elevation is also seen in F3 (Fig. 12e) but not clearly in F2 (Fig. 12c). The other three components, BLN, BLZ, and BRN, also exhibit this common behavior (Figs. S6, S7a–c). In BRZ, however, the ~12-hr acceleration of vibration is found in all modes (R1–R3, Fig. S7d–f). The less significant temporal variation in F2 requires further investigation for the possible mechanism.

The temperature and wind velocity data were processed in the same way as the seismic data, and the hourly variation of the atmospheric conditions can be seen in Figure 12b,d. The gradual increase of temperature and wind velocity, although moderate, appears to occur from ~8 a.m. to 9 p.m. with the maximum values being reached from 11 a.m. to 2 p.m. for temperature and 1 p.m. to 4 p.m. for wind velocity. A close look at Figure S3 shows that the strong wind did not arrive at the same hour of the day. The temporal variation of meteorological conditions may thus not fully explain the stable high amplitude from 9 a.m. to 9 p.m. seen in F1 and F3 in Figure 12a,e. The opening hours of TAIPEI 101 are from 11 a.m. to 9:30 p.m., and machinery operation may start or end a few hours earlier or later, so we cannot entirely rule out the influence of mechanical sources and human induced loading on the building. To better understand the role of mobility in the hourly variation of vibration amplitude for F1, we have requested one-day security measures in TAIPEI 101 for the people counts in every entryway. Entrance counter of TAIPEI 101 only monitors the employees with permit to enter the offices, not the visitors or tourists. On 6 July 2022, when the mobility data are available, the F1 amplitude variation is compared with people counts. As shown by the black line in Figure 12f, the abrupt increase in employee entrance occurred from 8 to 10 a.m. and stayed at the high level until 6 p.m. The F1 amplitude (red line) on the other hand, gradually rose around 8 a.m. and reach the top at noon and stayed at high level until 9 p.m. In visual inspection, the time period for relatively high F1 amplitude (9 a.m.–9 p.m.) is similar with the period of high mobility (9 a.m.–6 p.m.). The visitors and tourists not counted in the mobility record and the operation of the heating and cooling system in the building may add some uncertainties into the vibration amplitude–mobility correlation illustrated in Figure 12f.

Using the sensors on B5F and 74F and the broadband station located 1 km away, Chen *et al.* (2022) found that the >2 Hz ground vibration induced by traffic flow also showed a greater amplitude during the same time. They proposed that the resonance frequency of the soft sediment in the Taipei basin (0.4–1.8 Hz) allows the traffic signals to be preserved over a distance of 1 km and is therefore responsible for the continuous and stable acceleration of TAIPEI 101 for ~12 hr.

The hourly small vibration caused by the weather conditions or human activity may be able to activate cracks and thus change the modal frequency of the building. Polarity analysis using the data from the different sites in the building is needed to further investigate how severely the external conditions impact the vibration of the building compared with the internal conditions.

DISCUSSION AND CONCLUSIONS

Natural vibration characteristics of buildings under ambient condition

A better understanding of how building's natural frequencies are affected by environmental factors plays an essential role in building monitoring and structure health assessment. Table 2 summarizes the natural vibration characteristics of the buildings under ambient condition in recent years. We aim to highlight that the current study is able to establish higher modes of translational and rotational motions (F1–F3, R1–R3) for both the long- (seasonal and annual) and short-term (diurnal) vibration behavior in the high-rise building. Subsequently, we will briefly review the key findings in the example studies listed in Table 2.

The long- and short-term variation of fundamental frequencies under changing weather conditions is well documented by Clinton *et al.* (2006). Using 36 yr of data recorded in two buildings, they established the remarkable drop in frequencies with increasing amplitude of shaking from weak to strong motions. The long-term change of fundamental frequencies is ≤3% (increase) and −3% (drop) during the heavy rain and strong winds, respectively. They also noted that torsional mode is more sensitive to temperature and the translational mode because the maximum diurnal variation ≤3% during hot weather. Assuming the mass has not changed significant during the long study period, then the observed change in natural frequencies is mainly the result of decreasing stiffness of the system caused by soil saturation or wetting of the concrete. Herak and Herak (2010) also explored the long-term wander of the fundamental frequency with temperature, precipitation, and humidity using 19 months of continuous data. The observed seasonal variation in precipitation coincides with the variation in frequencies, which could be controlled by the degree of soil saturation and air temperature.

Applying RDT on one-month data from three buildings in France, Mikael *et al.* (2013) demonstrated the long-term frequency wanders that shows positive correlation between F1 and temperature. The correlation between F1 and wind, however, is not obvious because of a lack of strong atmospheric events. Using near 2-yr continuous data from building in Spain, García-Palacios *et al.* (2016) established the dependency of F1 on temperature and humidity. The temperature and humidity are responsible for 43.5% and 3.2% of the total variation in frequency, respectively. Guéguen *et al.* (2016) explored the long-term vibration behavior in a 66 m high-rise building that the meteorological forcing tends to induce dynamical motion and cause softening effect of the building. The correlation between strain and displacement on top of the building from five earthquakes is also discussed for improving the characterization of the seismic response and the assessment of the postearthquake integrity. Using 1448 earthquakes within the 16-yr period, Astorga *et al.* (2018) showed different event magnitude corresponding to different recovery rate, which reflects various level of material heterogeneity. They suggested that the log-time slope of recovery after the earthquake could be considered as a proxy of building health. The studies of long-term variation of buildings' vibrations, however, were solely focusing on the fundamental frequency F1.

TABLE 2
Comparison of Natural Frequencies Characteristics between Different Buildings under Ambient Condition

Building	Study Period	Sensors	Modes	Temperature	Wind	Amplitude	Data	Long Term	Short Term	References
43.9 m RC building, United States	36 yr	Translational	F1, F2, and R1	V	V	V	Continuous (hourly) +17 earthquakes	V	V	Clinton *et al.* (2006)
4-floor RC building, Croatia	19 months	Translational	F1	V	V	V	Continuous (hourly)	V	X	Herak and Herak (2010)
30-floor RC building, France	1 month	Translational	F1	V	V	X	Continuous (hourly)	V	X	Mikael *et al.* (2013)
17-floor RC building, Spain	800 days	Translational	F1	V	V	X	Continuous (hourly)	V	X	García-Palacios *et al.* (2016)
66 m steel structure building, United States	September–December 2004	Translational	F1	V	V	V	Continuous (hourly) +five earthquakes	V	X	Guéguen *et al.* (2016)
8-floor steel-framed RC building, Japan	1998–2014	Translational	F1	X	X	V	1448 earthquakes	V	X	Astorga *et al.* (2018)
13-floor RC building, France	1 day	Translational + Rotational	R1	V	V	X	Continuous (hourly)	X	V	Guéguen *et al.* (2021)
8-floor steel-framed RC building, Japan	1998–2018	Rotational	R1	X	X	X	1630 Earthquakes	V	X	Guéguen *et al.* (2021)
101 floors SRC building, Taiwan	1 yr	Translational + Rotational	F1∼F3, R1∼R3	V	V	V	Continuous (hourly)	V	V	This study

As the rotational motion during strong (e.g., earthquakes) and weak motion (e.g., wind) increases the stresses in structures, the importance of the torsion response of buildings has been also established by taking advantage of the rotational sensors (Bernauer *et al.*, 2012; Castellani *et al.*, 2012; Guéguen *et al.*, 2021). Using 1630 earthquakes with a wide range of magnitudes and distances, Guéguen *et al.* (2021) established a simple linear relationship between rotational rate and acceleration of 0.716. Using 1-day continuous data, Guéguen *et al.* (2021) observed that during a local storm in which wind velocity increases 78% and temperature decreases 30%, the fundamental frequencies in both translation and rotation decreases ∼1%. They also showed that the array-derived rotation rates are underestimated when compared with the real rotation sensor. At the top of the building, the amplitude ratio between rotation and translation is 10–20 times larger than at the bottom.

Dependency of natural frequencies on temperature in rotational motion

In fact, the rotational response of a building has been long considered a major cause of seismic damage, whereas the design (symmetric or asymmetric), resonance frequency and site condition of the building are proposed to control the torsion effect (e.g., Dewell, 1925; Hodgson, 1925; Ulrich, 1936; Sargeant and Musson, 2009; Hinzen, 2012; Guéguen *et al.*, 2021). Because the contribution of such effect is more significant for a high-rise building (Castellani *et al.*, 2012), TAIPEI 101 offers new perspectives in terms of the influence of temperature on natural vibration characteristics, especially under weak motion.

Temperature is often regarded as a dominant factor influencing the structural response. A significant increase in natural frequencies with increasing temperature has been often observed and explained by the temporary increase in structural stiffness (e.g., closing of microcracks due to thermal expansion) in warmer conditions (Sohn, 2007; Saisi *et al*, 2015; Magalhães *et al.*, 2016; Gentile *et al.*, 2016). The rising temperature may degrade Young's modulus and/or change the boundary condition in the modern reinforced concrete structures (Xia *et al.*, 2012), resulting in the unexpected negative correlation between frequency and temperature. Such negative correlation is also observed in masonry buildings, in which the frozen ice crystals inside microcracks is melt under higher temperature, leading to decrease in structural stiffness (Kita *et al.*, 2019). In TAIEPI 101,

TABLE 3
Maximum, Minimum, and Averaged Values of the Frequency Variation in Each Component and Mode

Component	Mode	Maximum Variation (%)	Minimum Variation (%)	Average Variation (%)
BLE	F1	16.804	0.379	1.006
	F2	1.943	0.276	0.568
	F3	1.363	0.134	0.340
BLN	F1	27.360	0.444	2.771
	F2	2.183	0.272	0.630
	F3	1.071	0.189	0.472
BLZ	F1	16.204	0.357	0.859
	F2	1.762	0.225	0.627
	F3	1.171	0.166	0.357
BRN	F1	22.108	0.403	8.708
	F2	1.893	0.253	0.588
	F3	1.106	0.253	0.545
BRZ	R1	4.726	0.816	2.143
	R2	1.992	0.284	0.658
	R3	1.382	0.215	0.685

the 660-ton TMD is made of steel, installed at the center of the 88th floor and suspended from the 92nd floor by cables. The amplitude of TMD remains stably high from mid-May to late-September (Fig. S2), coinciding with warmer condition of a year (Fig. 9). This indicates a possible temperature effect on TMD. It is possible for the rods connecting the pendulum mass and eight primary hydraulic viscous dampers become relatively loose during warmer period, resulting in soften stiffness of the structure and therefore, decreasing frequency. Given that TMD acts as a vibration control of rotational inertia, it is expected to have the significant temperature effect on TMD in rotational motion instead of translational. Other than the role of TMD, the opposite trend of temperature versus natural frequencies could also occur depending on the internal stress condition, construction material properties (elastic modulus), dynamic of cracks inside the building, and local perturbation of soil foundation properties (e.g., Clinton *et al.*, 2006; Todorovska and Trifunac, 2008; Todorovska, 2009; Michel and Guéguen, 2010). Further investigation on the TMD dynamic and the aforementioned conditions under various temperatures can be planned for a better understanding of damage sensitive features and for the removal of temperature effects from building monitoring data.

Remarkable vibration features from TAIPEI 101

Using the one-year continuous data recorded on the 90th floor of TAIPEI 101, we characterized the long- and short-term variation of modal frequencies and explored the controlling factors. The installation of rotational seismometers in TAIPEI 101 provides a new insight into our understanding of torsional effects in the response of such high-rise building. Given that the modal frequencies (F1–F3 and R1–R3) have never been explored in the worldwide buildings (Table 2), this study sets the first example for different behavior of translation versus rotation, fundamental versus higher modes, seasonal versus daily cycles, under the influence of shaking amplitude, weather conditions, and human activity inside the building. In Table 3, the maximum, minimum, and averaged variations of modal frequencies at different components and modes are summarized. The percentage in Table 3 is computed by hourly maximum (or minimum or average) subtracting daily average and being divided by daily average. At each component, the change in frequencies is largest for fundamental mode. The maximum variation ranges from 4.7% to 27.4%, and the averaged variation ranges from 0.9% to 8.7%. The second and third modal frequencies, however, changed only 1%. After the 2011 **M** 9.0 Tohoku earthquake, the maximum increase of frequency was ~3%–12% and 13%–33% at two buildings (ANX and THU) located in the epicentral area, respectively (Astorga and Guéguen, 2020). After the 1971 M 6.6 San Fernando earthquake, a permanent decrease of frequencies ranging from 7% to 17% was observed in Millikan Library without structural damage (Clinton *et al.*, 2006). This suggests that the fundamental frequencies of TAIPEI 101 varied significantly with weather conditions, which is comparable to the buildings' response to a large local earthquake. Although the seismic effect on fundamental frequencies differs between buildings, soil conditions, and source properties, the significant contribution of frequency variation from the environment should be taken into account for future monitoring of building health.

Translation versus rotation and fundamental versus higher modes. Using the RDT, accurate measurements of the modal frequencies were obtained because the coefficient of variation was confined in the range 0.14–0.46 for the translational components and 0.18–0.70 for the rotational components. We found that the first three modal frequencies (F1–F3) in translational motion (BLx) are nearly identical to those for the horizontal components of rotational motion (BRE and BRN) at 0.15 Hz, 0.43 Hz, and 0.78 Hz, respectively, but not for the vertical component of rotational motion BRZ (0.23 Hz, 0.59 Hz, and 0.93 Hz for R1–R3, respectively). This suggests that characteristics of the translational motion can be detected by the horizontal components of the rotational sensor, but the vertical component of the rotational seismograms exhibits distinct spectral behavior, reflecting a different driving mechanism.

The correlation between the modal frequencies and weather parameters suggests that (1) the temperature, absolute humidity, and air pressure are interconnected, and that there is a seasonal trend, (2) the wind velocity is not necessarily correlated with these three parameters, and (3) the earlier two groups of parameters are able to modulate the natural frequency of the translational and rotational motion of TAIPEI 101. In general, the three different frequency modes exhibit fairly similar relationships between frequency and

weather parameters. The wind velocity tends to have a consistently high correlation with the modal frequencies for all components. The temperature, however, appears to have a strong influence on the modal frequencies in both translational and rotational motion but with the opposite trends. In translational motion, the frequencies increase with rising temperature, but in rotational motion, the frequency–temperature relation is more complicated and not consistent at different components. As shown in Figure 8, the modal frequencies at BRN reveal positive correlation with temperature, but the ones at BRZ exhibits negative frequency–temperature correlation. This suggests that the temperature effect in the building acts differently for rotational and translational motion. As previously discussed in the Dependency of natural frequencies on temperature in rotational motion section, we argue that the heating effect of TMD may play a role on adjusting the F1 response during the warm weather.

In addition, we found a logarithmic relationship between the frequency and amplitude for all components and modes, indicative of the influence of amplitude on the natural frequency of the building. Compared with the higher modes (F2 and F3), the primary frequency F1 has a weaker dependency on the amplitude in both translation and rotation. This difference was commonly observed in other components and suggests a common mechanism behind the amplitude reduction of primary frequency, which may be associated with the modulation of the TMD system in TAIPEI 101.

Long-term versus short-term cycles. Different from the seasonal behavior that shows strong dependency with natural condition in temperature and wind velocity, the hourly variation of natural frequencies is likely controlled by different factors. When the amplitude of the data for the whole year was segmented into 24-hr-long windows to examine the short-term behavior, an amplitude elevation that lasted for >12 hr was clearly observed. Although the temperature and wind velocity appeared to rise during the same approximate period of time, their temporal variation did not match the stable high-amplitude vibration of the building from 9 a.m. to 9 p.m. Because the maximum temperature usually occurred around noon, and the strong winds did not arrive at the same hour of the day, we argue that external forces from (1) machinery vibration that occurs from before the building opening hour to after the closing hour and (2) the traffic in the immediate neighborhood, coupled with the effect of the meteorological conditions that reach their maximum influence around noon, were responsible for the 12-hr elevation of amplitude in TAIPEI 101. By assessing and separating the contribution of temperature, wind velocity, and human activities, the findings of this study require further investigation into the dynamic and continuous interaction between weather conditions, traffic flow, soil property, human activities, and building vibration.

DATA AND RESOURCES

The supplemental material includes seven figures showing the association between weather parameters (Figs. S1, S3), the possible controls of vibration amplitude at different frequency modes and components (Figs. S2, S4–S6), and the relationship of the amplitude in translation versus rotation motions (Fig. S7). The seismic data from the building array of TAIPEI 101 were provided by the research team in Institute of Earth Sciences, Academic Sinica, Taiwan, which has been led by the coauthor Bor-Shouh Huang and not released to the public. The weather data at the surface stations near TAIEPI 101 can be requested through the Central Weather Bureau (CWB) website (https://opendata.cwb.gov.tw/userLogin). ObsPy for seismic data processing is provided by https://docs.obspy.org. All websites were last accessed in January 2023.

DECLARATION OF COMPETING INTERESTS

The authors confirm that there are no known conflicts of interest associated with this publication, and there has been no significant financial support for this work that could have influenced its outcome.

ACKNOWLEDGMENTS

This collaborative work was initiated by the Dragon-Gate project funded by Taiwan MOST Grant Numbers 107-2911-I-003-507 and 108-2911-I-003-502. It is now supported by Taiwan NSTC Grant Number 111-2116-M-003-008-MY3. The authors wish to thank Benjamin Fong Chao, Wen-Tzong Liang, and Wan-Ru Huang for the helpful discussions and suggestions. The authors would like to thank Uni-edit (www.uni-edit.net, last accessed December 2022) for editing and proofreading this article.

REFERENCES

Astorga, A., and P. Guéguen (2020). Structural health building response induced by earthquakes: Material softening and recovery, *Eng. Rep.* **2,** no. 9, e12228, doi: 10.1002/eng2.12228.

Astorga, A., P. Guéguen, and T. Kashima (2018). Nonlinear elasticity observed in buildings during a long sequence of earthquakes, *Bull. Seismol. Soc. Am.* **108,** no. 3, 1185–1198, doi: 10.1785/0120170289.

Astorga, A. L., P. Guéguen, J. Rivière, T. Kashima, and P. A. Johnson (2019). Recovery of the resonance frequency of buildings following strong seismic deformation as a proxy for structural health, *Struct. Health Monit.* **18,** nos. 5/6, 1966–1981, doi: 10.1177/1475921718820770.

Au, S. K., F. L. Zhang, and P. To (2012). Field observations on modal properties of two tall buildings under strong wind, *J. Wind Eng. Ind. Aerodynam.* **101,** 12–23, doi: 10.1016/j.jweia.2011.12.002.

Bernauer, F., J. Wassermann, and H. Igel (2012). Rotational sensors-a comparison of different sensor types, *J. Seismol.* **16,** no. 4, 595–602, doi: 10.1007/s10950-012-9286-7.

Brossault, M. A., P. Roux, and P. Guéguen (2018). The fluctuation–dissipation theorem used as a proxy for damping variations in real engineering structures, *Eng. Struct.* **167,** 65–73, doi: 10.1016/j.engstruct.2018.04.012.

Castellani, A., M. Stupazzini, and R. Guidotti (2012). Free-field rotations during earthquakes: Relevance on buildings, *Earthq. Eng. Struct. Dynam.* **41,** no. 5, 875–891, doi: 10.1002/eqe.1163.

Chen, K. G., J. H. Wang, B. S. Huang, C. C. Liu, and W. G. Huang (2012). Vibrations of the TAIPEI 101 skyscraper caused by the 2011 Tohoku earthquake, Japan, *Earth Planets Space* **64,** no. 12, 1277–1286, doi: 10.5047/eps.2012.04.004.

Chen, K. C., J. H. Wang, B. S. Huang, C. C. Liu, and W. G. Huang (2013). Vibrations of the TAIPEI 101 skyscraper induced by typhoon Fanapi in 2010, *Terr. Atmos. and Ocean. Sci.* **24,** no. 1, 1–10, doi: 10.3319/TAO.2012.09.17.01(T).

Chen, K. H., T. C. Yeh, Y. Chen, C. W. Johnson, C. H. Lin, Y. C. Lai, M. H. Shih, P. Guéguen, W. G. Huang, B. S. Huang, *et al.* (2022). Characteristics and impact of environmental shaking in the Taipei metropolitan area, *Sci. Rep.* **12,** no. 1, doi: 10.1038/s41598-021-04528-6.

Clinton, J. F., S. C. Bradford, T. H. Heaton, and J. Favela (2006). The observed wander of the natural frequencies in a structure, *Bull. Seismol. Soc. Am.* **96,** no. 1, 237–257, doi: 10.1785/0120050052.

Cole, H. A. (1968). On-the-line analysis of random vibration, doi: 10.2514/6.1968-288.

Crouse, C. B., and P. C. Jennings (1975). Soil-structure interaction during the San Fernando earthquake, *Bull. Seismol. Soc. Am.* **65,** no. 1, 13–36, doi: 10.1785/bssa0650010013.

Dewell, H. D. (1925). Report of committee on building for safety against earthquakes, *Bull. Seismol. Soc. Am.* **15,** no. 3, 175–195, doi: 10.1785/bssa0150030175.

Douglas, B. M., and T. E. Trabert (1973). Coupled torsional dynamic analysis of a multistory building, *Bull. Seismol. Soc. Am.* **63,** no. 3, 1025–1039, doi: 10.1785/bssa0630031025.

Farrar, C. R., and K. Worden (2007). An introduction to structural health monitoring, *Phil. Trans. Roy. Soc. Lond. A* **365,** no. 1851, 303–315, doi: 10.1098/rsta.2006.1928.

Fu, J. Y., Q. S. Li, J. R. Wu, Y. Q. Xiao, and L. L. Song (2008). Field measurements of boundary layer wind characteristics and wind-induced responses of super-tall buildings, *J. Wind Eng. Ind. Aerodynam.* **96,** nos. 8/9, 1332–1358, doi: 10.1016/j.jweia.2008.03.004.

Fukuwa, N., R. Nishizaka, S. Yagi, K. Tanaka, and Y. Tamura (1996). Field measurement of damping and natural frequency of an actual steel-framed building over a wide range of amplitudes, *J. Wind Eng. Ind. Aerodynam.* **59,** 325–347.

García-Palacios, J., J. M. Soria, I. M. Díaz, and F. Tirado-Andrés (2016). Modal tracking with only a few of sensors: Application to a residential building, *8th European Workshop on Structural Health Monitoring, EWSHM 2016*, 3 (July), 1694–1704.

Gentile, C., M. Guidobaldi, and A. Saisi (2016). One-year dynamic monitoring of a historic tower: Damage detection under changing environment, *Meccanica* **51,** no. 11, 2873–2889, doi: 10.1007/s11012-016-0482-3.

Guéguen, P., and A. Astorga (2021). The torsional response of civil engineering structures during earthquake from an observational point of view, *Sensors* **21,** no. 2, 1–21, doi: 10.3390/s21020342.

Guéguen, P., F. Guattari, C. Aubert, and T. Laudat (2021). Comparing direct observation of torsion with array-derived rotation in civil engineering structures, *Sensors* **21,** no. 1, 1–17, doi: 10.3390/s21010142.

Guéguen, P., P. Johnson, and P. Roux (2016). Nonlinear dynamics induced in a structure by seismic and environmental loading, *J. Acoust. Soc. Am.* **140,** no. 1, 582–590, doi: 10.1121/1.4958990.

He, Y. C., and Q. Li (2014). Dynamic responses of a 492-m-high tall building with active tuned mass damping system during a typhoon, *Struct. Control Health Monitor.* **21,** no. 5, 705–720, doi: 10.1002/stc.1596.

Herak, M., and D. Herak (2010). Continuous monitoring of dynamic parameters of the DGFSM building (Zagreb, Croatia), *Bull. Earthq. Eng.* **8,** no. 3, 657–669, doi: 10.1007/s10518-009-9112-y.

Hillers, G., N. Graham, M. Campillo, S. Kedar, M. Landés, and N. Shapiro (2012). Global oceanic microseism sources as seen by seismic arrays and predicted by wave action models, *Geochem. Geophys. Geosys.* **13,** no. 1, doi: 10.1029/2011GC003875.

Hinzen, K. G. (2012). Rotation of vertically oriented objects during earthquakes, *J. Seismol.* **16,** no. 4, 797–814, doi: 10.1007/s10950-011-9255-6.

Hodgson, E. A. (1925). The St. Lawrence earthquake, February 28, 19251, *Bull. Seismol. Soc. Am.* **15,** no. 2, 84–99, doi: 10.1785/bssa0150020084.

Hua, X. G., Y. Q. Ni, J. M. Ko, and K. Y. Wong (2007). Modeling of temperature–frequency correlation using combined principal component analysis and support vector regression technique, *J. Comput. Civil Eng.* **21,** no. 2, 122–135, doi: 10.1061/(asce)0887-3801(2007)21:2(122).

Jeary, A. P. (1986). Damping in tall buildings—A mechanism and a predictor, *Earthq. Eng. Struct. Dynam.* **14,** no. 5, doi: 10.1002/eqe.4290140505.

Jeary, A. P. (1997). Damping in structures, *J. Wind Eng. Ind. Aerodynam.* **72,** 345–355.

Jennings, P. C., and J. H. Kuroiwa (1968). Vibration and soil-structure interaction tests of a nine-story reinforced concrete building, *Bull. Seismol. Soc. Am.* **58,** no. 3, 891–916, doi: 10.1785/bssa0580030891.

Kita, A., N. Cavalagli, and F. Ubertini (2019). Temperature effects on static and dynamic behavior of Consoli Palace in Gubbio, Italy, *Mech. Syst. Sig. Process.* **120,** 180–202, doi: 10.1016/j.ymssp.2018.10.021.

Lai, L. W. (2018). The influence of urban heat island phenomenon on PM concentration: An observation study during the summer half-year in metropolitan Taipei, Taiwan, *Theor. Appl. Climatol.* **131,** nos. 1/2, 227–243, doi: 10.1007/s00704-016-1975-7.

Li, Q. S., L.-H. Zhi, A. Y. Tuan, C.-S. Kao, S.-C. Su, and C.-F. Wu (2011). Dynamic behavior of Taipei 101 Tower: Field measurement and numerical analysis, *J. Struct. Eng.* **137,** no. 1, 143–155, doi: 10.1061/(asce)st.1943-541x.0000264.

Lin, C. J., W. G. Huang, H. P. Huang, B. S. Huang, C. S. Ku, and C. C. Liu (2012). Investigation of array-derived rotation in TAIPEI 101, *J. Seismol.* **16,** no. 4, 721–731, doi: 10.1007/s10950-012-9306-7.

Liu, C. C., B. S. Huang, W. H. K. Lee, and C. J. Lin (2009). Observing rotational and translational ground motions at the HGSD station in Taiwan from 2007 to 2008, *Bull. Seismol. Soc. Am.* **99,** no. 2B, 1228–1236, doi: 10.1785/0120080156.

Luco, J. E., M. D. Trifunac, and H. L. Wong (1987). On the apparent change in dynamic behavior of a nine-story reinforced concrete building, *Bull. Seismol. Soc. Am.* **77,** no. 6, 1961–1983, doi: 10.1785/bssa0770061961.

Magalhães, S. M. C., V. M. S. Leal, and I. M. Horta (2016). Predicting and characterizing indoor temperatures in residential buildings: Results from a monitoring campaign in Northern Portugal, *Energy Build.* **119,** 293–308, doi: 10.1016/j.enbuild.2016.03.064.

Martakis, P., Y. Reuland, and E. Chatzi (2022). Amplitude dependency effects in the structural identification of historic masonry

buildings, *Lecture Notes in Civil Engineering, 200 LNCE*, 140–147, doi: 10.1007/978-3-030-91877-4_17.

Meli, R., E. Faccioli, D. Muria-Vila, R. Quaas, and R. Paolucci (1998). A study of site effects and seismic response of an instrumented building in Mexico city, *J. Earthq. Eng.* **2,** no. 1, 89–111, doi: 10.1080/13632469809350315.

Michel, C., and P. Guéguen (2010). Time-frequency analysis of small frequency variations in civil engineering structures under weak and strong motions using a reassignment method, *Struct. Health Monitor.* **9,** no. 2, 159–171, doi: 10.1177/1475921709352146.

Mikael, A., P. Guéguen, P. Y. Bard, P. Roux, and M. Langlais (2013). The analysis of long-term frequency and damping wandering in buildings using the random decrement technique, *Bull. Seismol. Soc. Am.* **103,** no. 1, 236–246, doi: 10.1785/0120120048.

Mordret, A., H. Sun, G. A. Prieto, M. N. Toksöz, and O. Büyüköztürk (2017). Continuous monitoring of high-rise buildings using seismic interferometry, *Bull. Seismol. Soc. Am.* **107,** no. 6, 2759–2773, doi: 10.1785/0120160282.

Nayeri, R. D., S. F. Masri, R. G. Ghanem, and R. L. Nigbor (2008). A novel approach for the structural identification and monitoring of a full-scale 17-story building based on ambient vibration measurements, *Smart Mater. Struct.* **17,** no. 2, doi: 10.1088/0964-1726/17/2/025006.

Saisi, A., C. Gentile, and M. Guidobaldi (2015). Post-earthquake continuous dynamic monitoring of the Gabbia Tower in Mantua, Italy, *Constr. Build. Mater.* **81,** 101–112, doi: 10.1016/j.conbuildmat.2015.02.010.

Sargeant, S. L., and R. M. W. Musson (2009). Rotational earthquake effects in the United Kingdom, *Bull. Seismol. Soc. Am.* **99,** no. 2B, 1475–1479, doi: 10.1785/0120080097.

Sohn, H. (2007). Effects of environmental and operational variability on structural health monitoring, *Phil. Trans. Roy. Soc. Lond. A* **365,** no. 1851, 539–560, doi: 10.1098/rsta.2006.1935.

Song, M., B. Moaveni, C. Papadimitriou, and A. Stavridis (2019). Accounting for amplitude of excitation in model updating through a hierarchical Bayesian approach: Application to a two-story reinforced concrete building, *Mech. Syst. Sig. Process.* **123,** 68–83, doi: 10.1016/j.ymssp.2018.12.049.

Stehly, L., M. Campillo, and N. M. Shapiro (2006). A study of the seismic noise from its long-range correlation properties, *J. Geophys. Res.* **111,** no. 10, doi: 10.1029/2005JB004237.

Tamura, Y., and S. Y. Suganuma (1996). Evaluation of amplitude-dependent damping and natural frequency of buildings during strong winds, *J. Wind Eng. Ind. Aerodynam.* **59,** nos. 2/3, 115–130, doi: 10.1016/0167-6105(96)00003-7.

Todorovska, M. I. (2009). Soil-structure system identification of Millikan Library North-South response during four earthquakes (1970-2002): What caused the observed wandering of the system frequencies? *Bull. Seismol. Soc. Am.* **99,** no. 2A, 626–635, doi: 10.1785/0120080333.

Todorovska, M. I., and M. D. Trifunac (2007). Earthquake damage detection in the Imperial County Services Building I: The data and time-frequency analysis, *Soil Dynam. Earthq. Eng.* **27,** no. 6, 564–576, doi: 10.1016/j.soildyn.2006.10.005.

Todorovska, M. I., and M. D. Trifunac (2008). Impulse response analysis of the Van Nuys 7-storey hotel during 11 earthquakes and earthquake damage detection, *Struct. Control Health Monitor.* **15,** no. 1, 90–116, doi: 10.1002/stc.208.

Tuan, A. Y., and G. Q. Shang (2014). Vibration control in a 101-storey building using a tuned mass damper, *J. Appl. Sci. Eng.* **17,** no. 2, 141–156, doi: 10.6180/jase.2014.17.2.05.

Ulrich, F. P. (1936). Helena earthquakes, *Bull. Seismol. Soc. Am.* **26,** no. 4, 323–339, doi: 10.1785/bssa0260040323.

Vidal, F., M. Navarro, C. Aranda, and T. Enomoto (2014). Changes in dynamic characteristics of Lorca RC buildings from pre- and post-earthquake ambient vibration data, *Bull. Earthq. Eng.* **12,** no. 5, 2095–2110, doi: 10.1007/s10518-013-9489-5.

Xia, Y., B. Chen, S. Weng, Y. Q. Ni, and Y. L. Xu (2012). Temperature effect on vibration properties of civil structures: A literature review and case studies, *J. Civil Struct. Health Monitor.* **2,** no. 1, 29–46, doi: 10.1007/s13349-011-0015-7.

Manuscript received 18 July 2022
Published online 20 January 2023